Green synthesis and photocatalytic activity of nickel oxide nanostructures in the degradation of organic dyes

D. Princess Jeba[1], T. Peter Amaladhas[1]*
PG and Research Department of Chemistry, V.O. Chidambaram College, Tuticorin -628008   Affiliated to
Manonmaniam Sundaranar University, Abishekapatti, Tirunelveli, Tamil nadu, India
Email: dprincessjeba@gmail.com, peteramaladhas@gmail.com

Abstract- NiO nanoparticles were synthesized by a facile and green biological method using *Pisonia alba* leaf extract. The biomolecules present in the extract acts as complexing as well as capping agent. The morphological, structural, and optical properties of this catalyst were analyzed using XRD, EDAX, TEM and UV–vis spectroscopy. The photocatalytic degradation of methylene blue (MB) has been investigated using NiO catalysts under visible light irradiation in aqueous solutions. The effects of solution pH, H_2O_2 concentration, initial MB concentration, catalyst dosage and light intensity on the degradation of MB have been systematically investigated. The rate of the reduction/degradation was found to increase with increasing amount of the photocatalyst, which could be attributed to higher dispersity, and small size of the nanoparticles. These results will be useful for future improvement of active heterogeneous photo-Fenton catalysts for organic dye-containing wastewater treatments.

Index Terms-photocatalyst; semiconductor; nickel oxide nanoparticles; *Pisonia alba*

1. INTRODUCTION

Nanostructured materials have attracted intense attention due to their amazing physical and chemical properties. Among the various types of nanomaterials, nanostructured transition metal oxides deserve special consideration for their outstanding properties and technological applications. The nanomaterials having unique properties are used in various applications, such as photocatalysis, lithium ion batteries, smart windows, field emission studies, antimicrobial activity, dye-sensitized photocathodes, thermal conductivity and anti-ferromagnetic films [1–4]. In recent research, nickel oxide nanoparticles have drawn a greater interest, because of its unique properties. It belongs to a wide band gap (3.6–4.0 eV) p-type semiconductor and is chemically stable with high electro-optical efficiency. Nickel oxide nanoparticles are widely applied in numerous fields as adsorbents, solar and fuel cells, catalytic agents, gas sensors, magnetic and antibacterial materials [5, 6]. Since particle size, morphology and high crystallinity influence the physiochemical properties; it is of great importance to synthesize NiO nanoparticles with small particle size, which could enhance the efficiency of their applications. However, synthesis of transition metal oxide nanoparticles with desired properties and having environmental stability is very difficult to achieve. Numerous methods to fabricate NiO NPs have been reported in the literature, which includes solvothermal [7], precipitation-calcination [8], chemical precipitation [9], microwave-assisted hydrothermal [10], and thermal decomposition [11] methods. These methods involve ample reactants and starting materials, draggy procedures and complex apparatus. These conventional methods possess high cytotoxicity, low productivity and are not ecofriendly. In the past few decades, bionanotechnology is gaining momentum, as the scheme includes nonhazardous, environmental friendly biological systems like bacteria, fungi, leaves, vitamins and yeast for the synthesis of metal oxide nanoparticles [12]. Therefore, recently environmental benign green chemistry approach is used to synthesize NiO NPs.

The increasing environmental pollution has attracted the worldwide researchers to work on the development of efficient photocatalysts based on semiconductors for the treatment of contaminated water resources by various organic pollutants that are released from many industries. They impart toxic damage to the environment, human body and aquatic life. Synthetic dyes in different industries such as leather treatment, dyeing of cloth, plastics, paper and pulp manufacturing, and printing have been used widely and could be a cause of environmental pollution. Particularly, dyes and pigments released from different industries with colour into the aquatic ecosystems poses serious ecological problem and are also the major issue of water pollution in the world today [13-15]. In addition to this, dyes such as methylene blue (MB), malachite green (MG) methyl orange (MO), and congo red (CR) are also high

toxicity, carcinogenic, and mutagenic organic compounds. Due to this reason, extensive researches have been done for the removal of organic pollutants to reduce the risks. However, the decolorization of wastewaters is still one of worldwide difficulty to which various technologies have been applied [16-18]. Recently, technological applications such as adsorption, photocatalytic degradation, chemical oxidation, membrane filtration, flocculation, and reduction have been used to remove organic pollutants and decolourize wastewaters [19–20]. Still now, the development of cost-effective, environmentally benign, and efficient techniques is an important concern in the field of environmental science. Recently the reduction of organic pollutants has been carried out by metal nanoparticles (like, Ag and Au) based catalysts. [21]. However, the use of precious metal nanoparticle makes the catalyst expensive. Moreover, the easy aggregation of metal nanoparticles limits their large-scale applications, and sometimes needs the catalyst support [22–24]. In order to avoid this problem, semiconductor materials could be used to treat organic pollutants containing wastewater [25]. Recently photocatalytic degradation using metal oxide semiconductors like ZnO, TiO_2, CuO and NiO has been suggested as the inexpensive method to remove the organic dyes and pollutants from waste water [26-27]. Among the semiconductors in nano regime, the unique features of NiO, like inexpensive, non-toxic, photo stability and easy availability make it to be an efficient photocatalyst for the degradation of various organic pollutants. Hence in the present work, NiO nanoparticles were prepared by a novel, simple, efficient, environment friendly and green route using *Pisonia alba* leaf extract, which plays the role of complexing and capping agent. Using leaf extract, it is possible to control the shape and size of the particles. Being biotemplates, the extract also hinders agglomeration of nanoparticles. The green synthesized nanoparticles were characterized by UV-Visible, IR, XRD, EDAX and TEM analysis. The photocatalytic behavior, effects of various operating parameters on the degradation of methylene blue by NiO nanoparticles were discussed. The plant *pisonia alba* (synonym: pisonia grandis, pisonia morindifolia) commonly known as Leechikottai kerai in Tamil. The plant *Pisonia alba* belonging to the family Nyctaginaceae, is an evergreen glaborous garden tree with young shoots are minutely puberulous. The phytochemical analysis of *P. alba* showed the presence of numerous bioactive components includes pinnatol, allantonin, β-sitosterol, α-sinasterol, β-sitosterol glucoside, octocosanal, dulcitol, flavonoids and quercetin. It is extensively used in Indian traditional medicine as an anti-diabetic, ant-inflammatory, wound healing, diuretic, analgesic, filariasis, dysentery and rheumatic disorders [28].

2. EXPERIMENTAL DETAILS

2.1. *Chemicals and reagents*

Methylene blue, H_2O_2 (30% w/w), $NiCl_2.6H_2O$ and NaOH were purchased from Merck, Mumbai. All chemicals were AR grade and used without further purification. Double distilled water was used for sample preparation. NaOH and H_2SO_4 were employed for pH adjustment.

2.2. *Preparation o f nickel oxide catalyst*

About 20g of fresh leaves of *Pisona alba* were collected, washed thoroughly with double distilled water, cut into fine pieces and boiled with 100 ml double distilled water in a beaker for 10 minutes. The extract was cooled to room temperature and filtered through Whatman filter paper No. 41. The pH of 10 ml of leaf extract was adjusted to 9 using 0.1N NaOH. 10 ml of Nickel chloride solution was mixed with pH adjusted leaf extract. The dark green colloid thus obtained was centrifuged at 13000 rpm, washed several times with distilled water and dried. The solid thus obtained was calcined at 773 K for 1 h.

2.3. *Characterization of catalyst*

The UV-Vis spectral analysis was performed on a JASCO, V-650 spectrophotometer. FT-IR spectra for the dry powder of leaves extract and nanoparticles were recorded with Thermoscientific, Nicolet iS5 spectrometer in the region of 400-4000 cm^{-1}. TEM analysis was done on PHILIPS, CM 200 instrument operated at 200 kV, resolution 2.4A. The crystal structure was analysed by a Panalytical X'Pert powder X'Celerator Diffractometer, with CuKα monochromatic filter. The elemental composition of the synthesized catalysts was analysed using EDX (JOEL Model JED-2300). The catalyst was sonicated using Enertech probe sonicator-Ultrasonic, Model: ENUP-500 A. The photocatalytic experiments were done by using Heber visible annular immersion type photoreactor, Model: HIPR-MP-400.

International Journal of Research in Advent Technology, Vol.6, No.11, November 2018
E-ISSN: 2321-9637
Available online at www.ijrat.org

2.4. *Photocatalytic degradation studies*

Photocatalytic activities of the synthesized nanoparticles were evaluated by monitoring the decolourization of aqueous solution of methylene blue dye. Blank experiments were carried out in visible light irradiation without H_2O_2, with catalyst in dark and without H_2O_2. The reaction vessel was made of a cylindrical borosilicate glass reactor (total capacity 90 mL) with 2.5 cm inner diameter and 35 cm height. A lamp was vertically placed in the middle of the reactor within a double-wall cooling system. The photocatalytic experiments were performed in a batch reactor using artificial visible light produced by a 150W lamp with a wavelength range of 300 to 800 nm to simulate sunlight. It was possible to achieve the required light intensity by changing the optical intensity. The reactor temperature was maintained at $29 \pm 2°C$ by circulating cool water and the mixture was stirred using a magnetic bar with a speed of 500 RPM. The photo Fenton activity was studied by changing the reaction parameters. Specifically, the H_2O_2 concentration was adjusted between 5×10^{-3} M and 10×10^{-3} M; the concentration of MB dye was between 1×10^{-5} M and 5×10^{-5} M, the catalyst loading was between 0.1and 0.3 g L^{-1}, the pH range was between 3 and 8, and the visible light intensity was between 150W and 500W.

The reactions were performed by adding the desired amount of H_2O_2 to a pH-adjusted solution that contained catalyst and different concentrations of MB. In addition, the initial solution pH was adjusted using 0.1 M H_2SO_4 or 0.1 M NaOH solution. At the beginning, the catalyst was added to MB solutions that were magnetically stirred, in dark conditions for 30 min to achieve the adsorption/desorption equilibrium between the dye and the photo-catalyst prior to H_2O_2 addition. During irradiation, 5 ml samples were withdrawn at pre-set time intervals and were centrifuged at 2000 rpm, and their absorbance was determined using a UV-Visible spectrophotometer.

3. RESULTS AND DISCUSSION

3.1. *UV-Vis-DRS Studies*

The UV-visible diffuse reflectance spectrum (DRS) of nickel oxide nanoparticles is shown in figure 1. The spectrum shows a strong band around 300 nm is attributed to the NiO exciton transition due to surface defects. The strongest absorption peak at around 377 nm is well pronounced in nano sized NiO. The peak is ascribed to the electronic transition from the valence band to the conduction band in the NiO semiconductor. The d−d transition is forbidden according to Laporte's rule, but because of spin−orbital interaction, it is weakly allowed [29-30]. For a direct type of semiconductor the optical band gap E_g could be derived from the optical absorption spectroscopy using Tauc's relationship, $(\alpha h\upsilon)^2 = B(h\upsilon - Eg)^n$. Where α is the absorption coefficient, $h\upsilon$ is the photon energy and A is a constant. A typical plot is shown in fig. 1 (inset). By fitting the linear part of the plot and extrapolating the linear region on the energy axis, the optical band gap or the exciton ground state energy of the NiO nanoparticles could be derived. The obtained band gap value, 3.25 eV is in agreement and within the values reported in the literature [31-34].
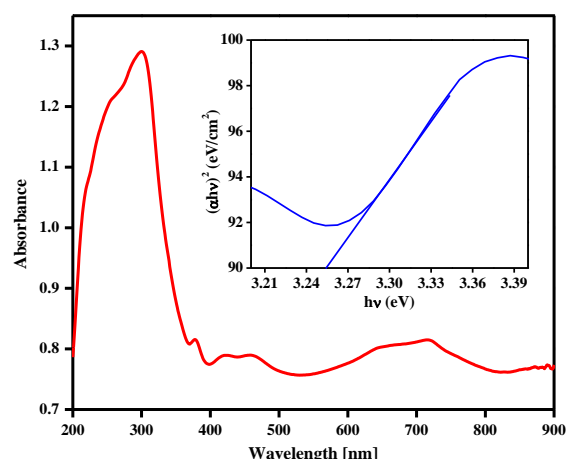

Fig. 1. UV-Vis-DRS spectrum of NiO nanoparticles (Inset: Plot of $\alpha h\upsilon^2$ vs $h\upsilon$).

3.2. *XRD Studies*

To evaluate the crystal properties of NiO nanoparticles, XRD was recorded and shown in figure 2. The diffraction pattern of NiO nanoparticles was well indexed with standard JCPDS card No. 01-175-0269, with face centered cubic phase at $2\theta = 37.18$, 43.26, 62.84 and 75.43 which can be perfectly related to (111), (200), (220) and (311) crystal planes [29, 32, 34, 35]. No evidence of secondary oxides such as, Ni_2O_2, Ni_2O_3 etc. were found from the XRD analysis, since there were no characteristic peaks with the respective standard JCPDS diffraction patterns.

International Journal of Research in Advent Technology, Vol.6, No.11, November 2018
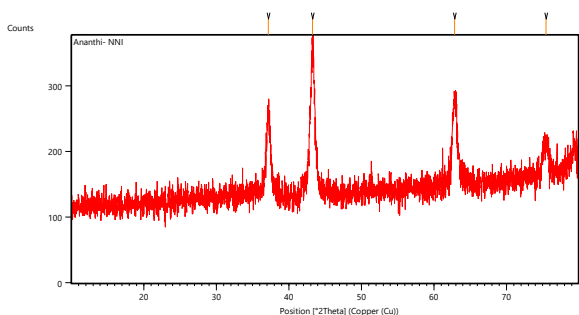*E-ISSN: 2321-9637*
Available online at www.ijrat.org

Fig. 2. XRD pattern of NiO nanoparticles.

The results also show that the synthesized NiO nanoparticles had a high purity, with the absence of impurity peaks. XRD analysis results were used to evaluate crystallite size of the obtained samples. The crystal size of the NiO nanoparticles was determined by the X-ray line broadening method using the Debye-Scherrer equation, $D = K\lambda/\beta\cos\theta$, where, D is the crystal size in nanometers, λ is the wave length of the radiation (1.54056Å for CuKα radiation), K is a shape constant equal to 0.94 and β is the peak width at half-maximum intensity and θ is the peak position. The crystallite size obtained from the preferentially oriented peak of (200) plane was found to be 14.2 nm.

3.3. EDAX Studies

The energy dispersive X-ray microanalysis was carried to investigate the chemical composition of NiO nanoparticles. Figure 3 shows the EDX pattern of NiO sample.
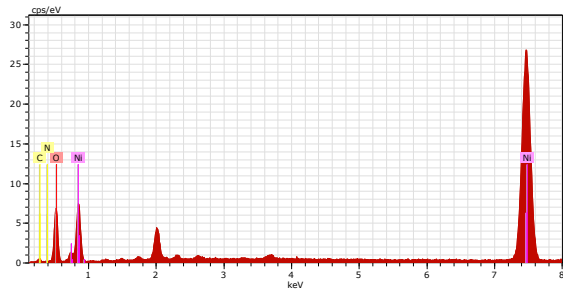

Fig. 3. EDAX spectrum of NiO nanoparticles.

This pattern shows the presence of both nickel (7.5 Kev) and oxygen (0.5 KeV) peaks and confirms the presence of NiO NPs. Traces of carbon, nitrogen and oxygen are also seen, which may be due to the presence of biomolecules as capping agent, derived from plant extract.
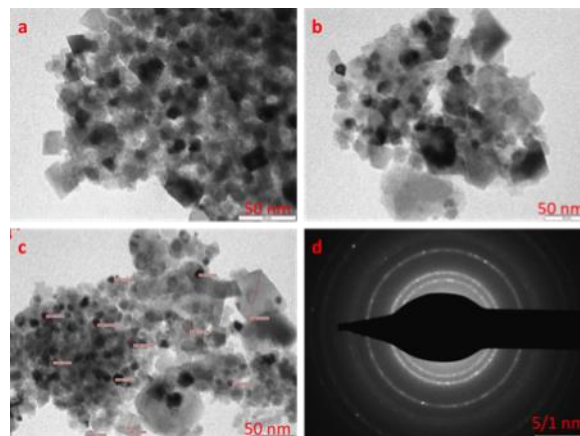
3.4. TEM Studies

Fig. 4. (a-d) TEM images and (d) SAED pattern of NiO nanoparticles.

The morphology of NiO was studied using transmission electron microscopy. The result is represented in Figure 4(a–d). From the TEM images it was found that the average particle size to be 10 ± 4 nm. The corresponding selected area electron diffraction (SAED) shows polycrystalline nature. The particle size was in the range of 10–14 nm and it agrees well with the average crystallite size calculated from the XRD pattern.

3.5. Photocatalytic degradation of methylene blue dye by nickel oxide nanoparticles

The photocatalytic activity of the biosynthesized NiO nanoparticles was assessed by monitoring the changes in the optical absorption spectra of MB solution. The degradation process involves photochemical reactions on the surface of the NiO nanoparticles. Hence an increase in the surface area of the photocatalyst leads to a greater degradation of the dye. The size and the dispersion of the photocatalyst in the solution play an important role in the degradation of dyes. Figure 5 shows the time dependent UV-visible spectra for degradation of MB dye using NiO nanoparticles as a photocatalyst under visible light irradiation.

International Journal of Research in Advent Technology, Vol.6, No.11, November 2018
E-ISSN: 2321-9637
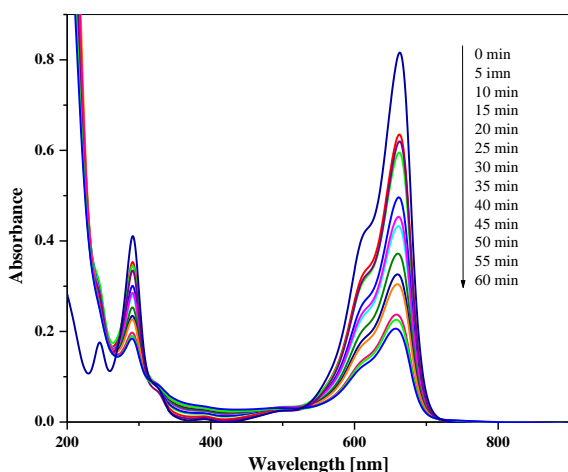*Available online at www.ijrat.org*

Fig. 5. Time dependent UV-visible spectra for degradation of MB dye using NiO nanoparticles as a photocatalyst under visible light irradiation. (pH = 6, $[H_2O_2] = 5\times10^{-3}$ M, 0.1 g L^{-1} catalyst, Light intensity = 150W).

UV-visible spectra of dye showed a strong absorption band at 663 nm. After the addition of H_2O_2 and irradiating with visible light to the MB and NiO nanoparticles equilibrated mixture, the absorption band intensity started decreasing with irradiation time. The intensity of the absorption band at 663 nm decreases with time and the color of the MB solution also fade away. This indicates the destruction of chromophoric structure of MB dye. The photodegradation reaction followed pseudo first order kinetics and the rate of the reaction can be obtained using the equation: ln C = - kt + ln C$_o$, where, k is the rate constant, C$_o$ and C are concentration before and after degradation of dye, respectively. The rate constant for photodegradation of MB dye can be calculated using the above equation.
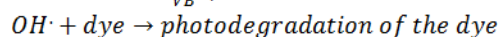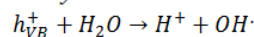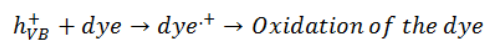
In the presence of photocatalyst, visible radiation and H_2O_2, more than 39% of dye got degraded after 60 min of irradiation while only 13.6 % degradation was observed in the presence of photocatalyst without irradiation and only 21.2 % degradation of the dye was observed in the absence of H_2O_2. These experiments demonstrate that, both visible light, H_2O_2 and a photocatalyst are essential for effective degradation of MB. When NiO nanoparticles are irradiated with the visible light, electrons get promoted from the valence band to the conduction band of the semiconducting oxide to give electron–hole pairs. The potential of the valence band (h_{VB}) is positive enough to generate hydroxyl radicals at the surface and the potential of the conduction band (e_{CB}) is negative enough to reduce molecular oxygen. The hydroxyl radical is a powerful oxidizing agent and attacks organic dyes present at or near the surface of photocatalyst. H_2O_2 is used as a source of OH$^\bullet$ produced during the catalytic breakdown. The hydrogen peroxide can accept the photogenerated electrons from the conduction band allowing the formation of the OH$^\bullet$ radicals that prevent the recombination of the charges and increasing the photocatalytic process [36].

On the surface of the catalyst the semiconductor is excited by a photon of light and an electron-hole pair is generated.

$$NiO + h\upsilon \rightarrow NiO(e^-_{CB} + h^+_{VB})$$
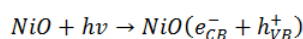
The valence band hole has a high oxidative potential producing the oxidation of the dye and generating the hydroxyl radical from the water molecule. Consecutive reactions allow the oxidation of the dye and the complete photodegradation:

$$h^+_{VB} + dye \rightarrow dye^{\cdot +} \rightarrow Oxidation\ of\ the\ dye$$
$$h^+_{VB} + H_2O \rightarrow H^+ + OH\cdot$$
$$h^+_{VB} + OH^- \rightarrow OH\cdot$$
$$OH\cdot + dye \rightarrow photodegradation\ of\ the\ dye$$

The conduction band electron ejected from the surface produces radicals of the oxygen molecule in the solution.

$$e^-_{CB} + O_2 \rightarrow O^-_2$$
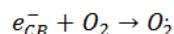
The oxygen radicals react with the hydrogen peroxide producing hydroxyl radical and ions. At the same time regenerate the O_2 to continue with the reaction [37, 38]

$$O^-_2 + H_2O_2 \rightarrow OH\cdot + OH^- + O_2$$
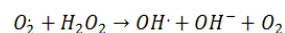
Owing to their ability to easily absorb some of visible light, another mechanism of photocatalytic dye degradation can also occur under visible light. This mechanism involves the dye excitation under visible light photon (l > 400 nm) from the ground state (Dye) to the triplet excited state (Dye*). This excited state dye species is further converted into a semi-oxidized radial cation (Dye$^{+\bullet}$) by an electron injection into the conduction band of NiO. [39] Due to reaction between these trapped electrons and dissolved $_\bullet$oxygen in the system superoxide radical anions (O$_2^{\ }$) are formed which in turn result into hydroxyl radicals (OH$^-$) formation. These (OH$^\bullet$) radicals are mainly responsible for the oxidation of the dye [40].

$$Dye + h\upsilon \rightarrow dye*$$
$$Dye* + NiO \rightarrow dye^+ + NiO^-$$
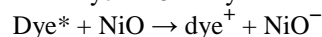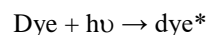
Since the band gap of nickel oxide falls under UV region, the visible light initiated dye sensitized mechanism is much more pronounced than semiconductor mechanism.

International Journal of Research in Advent Technology, Vol.6, No.11, November 2018
E-ISSN: 2321-9637
Available online at www.ijrat.org

The effect of various reaction parameters on the degradation of metylene blue was studied and was discussed below.

3.6.1. *Effect of initial MB concentration*

The effect of the dye concentration on the degradation of methylene blue was observed by maintaining all other parameters constant and varying the concentrations of dye from 1×10^{-5} to 5×10^{-5} M.
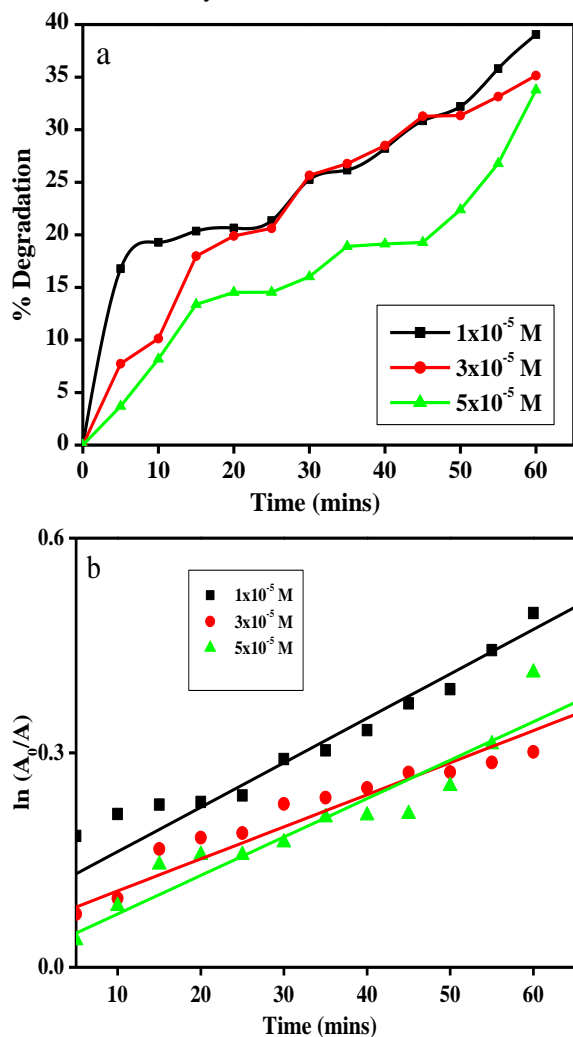

Fig. 6. a) Effect of dye concentration on degradation of MB, b) Rate of degradation at different dye concentration (pH = 6, $[H_2O_2]$ = 5×10^{-3} M, NiO = 0.1 gL^{-1}, Light intensity = 150W).

The results as reported in figure 6 indicate that increase in the dye concentration results in retardation of reaction. Before the irradiation to visible light, the adsorption of MB solutions with the photocatalyst was studied in dark condition with constant stirring for one hour, but the adsorption percentage was found to be 13.6%. The percentage of degradation under visible light irradiation was found to decrease with increase in dye concentration. The reason for this decrease is attributed to the shielding effect of dye at high concentration that hinders the penetration of light to the dye molecules deposited over the catalyst surface. At higher concentration more and more molecules of MB adsorbed on the surface of NiO photocatalyst, which have hinder the photo generation of hydroxyl radicals, which causes the decreasing rate of photo degradation reaction of the catalyst [41, 42]. The increased amounts of dye and reaction intermediates competed with both hydroxyl radicals and active reaction sites at the NiO surface. Hence, the fraction of hydroxyl radicals that attacked the dye molecules and its reaction intermediates declined as the dye concentration increased. Hence, further experiments were carried out with 1×10^{-5} M concentration of dye.

3.6.2. *Effect of pH of the solution*

The solution pH is a significant parameter in photocatalytic degradation process. The influence of different pH (3–8) value on the degradation efficiency of MB was investigated using 5 mg of photocatalyst in 50 mL of 1×10^{-5} M MB solution and the result is shown in figure 7. The natural pH value of 1×10^{-5} M MB solution was found to be ~ 6. The pH value was adjusted using dilute HCl or dilute NaOH solution for the experiment. The experimental results reveal that the percentage degradation of dye was found to be lower at lower pH values increases with increase in pH. The increase in rate of photocatalytic degradation might be due to the more availability of OH^- ions in alkaline medium, which will generate more OH radicals by combining with holes, which are formed due to the electronic excitation in catalyst [43]. For more alkaline solution pH (pH 10), it was observed a total decolorization of methylene blue within a few seconds. This is because, methylene blue dye changes to a colorless leuco compound at highly alkaline medium [44]. Hence, all further experiments were done at the natural pH of the dye solution.
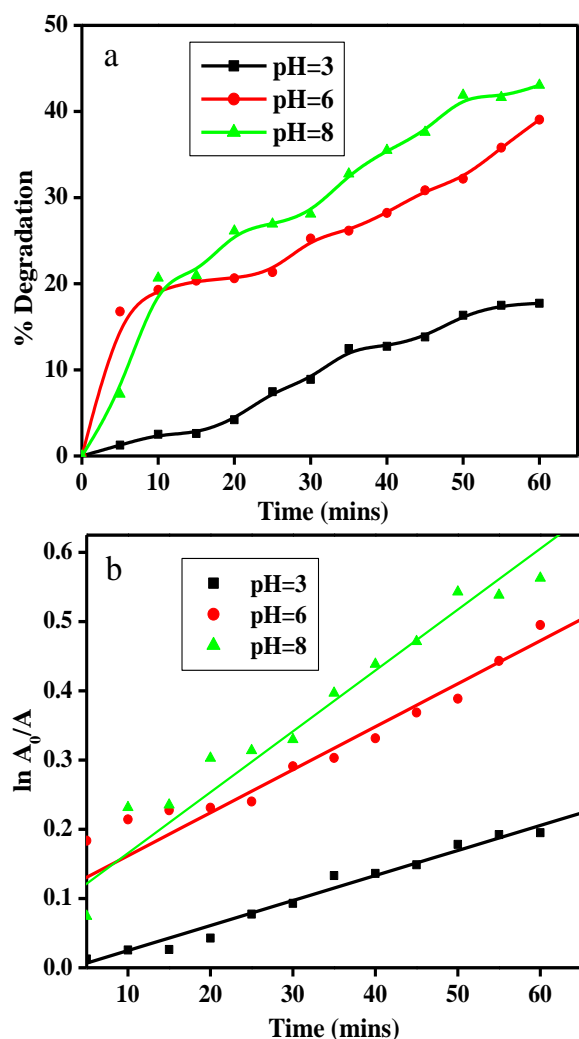
International Journal of Research in Advent Technology, Vol.6, No.11, November 2018
E-ISSN: 2321-9637
Available online at www.ijrat.org

Fig. 7. a) Effect of pH on degradation of MB, b) Rate of degradation of MB at different pH ([MB] = 1×10^{-5} M, [H_2O_2] = 5×10^{-3} M, NiO = 0.1 gL^{-1}, Light intensity = 150W).

Fig. 8. a) Effect of H_2O_2 concentration on degradation of MB, b) Rate of degradation of MB at different H_2O_2 concentration ([MB] = 1×10^{-5} M, pH = 6, NiO = 0.1 gL^{-1}, Light intensity = 150W).

3.6.3. *Effect of H2O2 concentration*

The impact of H_2O_2 concentration on the degradation of MB using NiO nanoparticles is shown in figure 8. The study was performed at different concentrations of H_2O_2 with all the other parameters kept constant. The concentration of H_2O_2 was varied from 5 mM to 10 mM. The results demonstrate that the degradation efficiency increased with an increase in H_2O_2 concentration. The addition of H_2O_2 to the heterogeneous system increases the concentration of OH radicals, since it inhibits the electron hole recombination [45].
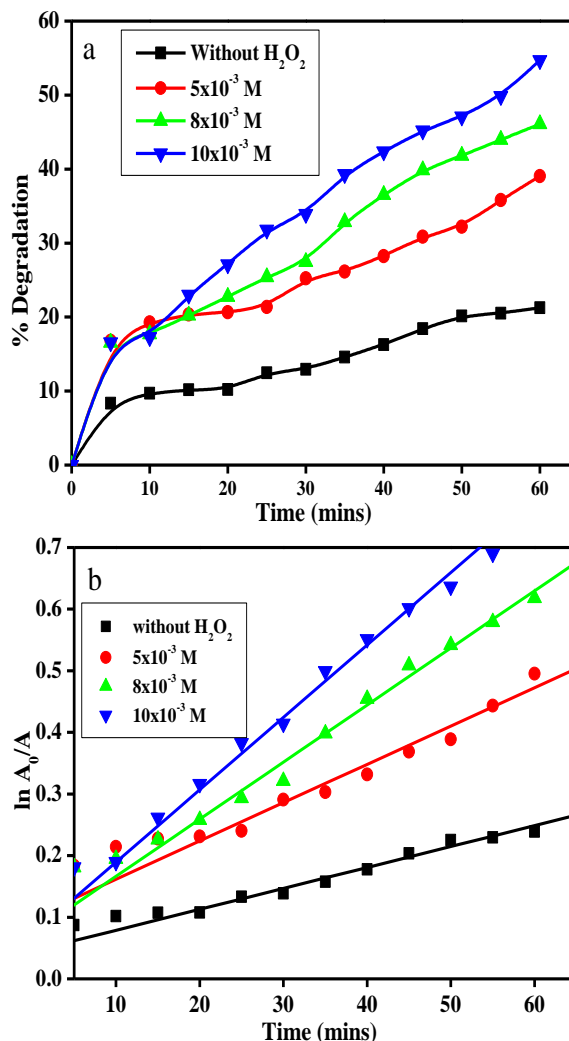
3.6.4. *Effect of catalyst dosage*

The effect of catalyst dosage on degradation of MB was studied at different dosages of catalyst with all the other parameters kept constant. The rate of decolorization of MB was significantly affected by the catalyst dosages. When the concentration of the catalyst was increased from 0.1 gL^{-1} to 0.3 gL^{-1}, the decolorization efficiency of MB increased almost linearly. Higher degradation efficiency was observed as the catalyst dosages were increased, which increased the active sites on the surface of the catalyst and generated free hydroxyl radicals [46].

International Journal of Research in Advent Technology, Vol.6, No.11, November 2018
E-ISSN: 2321-9637
Available online at www.ijrat.org

Fig. 9. a) Effect of catalyst dosage on degradation of MB, b) Rate of degradation of MB at different catalyst dosage ([MB] = 1×10^{-5} M, pH = 6, [H_2O_2] = 5×10^{-3} M, Light intensity = 150W).

3.6.5. *Effect of visible light intensity*

The influence of the light intensity on the decolorization of MB was examined in presence of NiO nanoparticles under visible light of different intensities (150 W, 300 W, and 500 W) and standard experimental conditions. The photo-degradation efficiency increased with an increase in irradiation time and illumination intensity of the light source. From figure 10, it is observed that the degradation efficiency of MB increased with an increase of artificial visible-light intensity from 150 W to 500 W. An increase in the light intensity will increase the number of photons striking per unit area per unit time of photo catalyst surface, which results in the generation of more hydroxyl radicals responsible for photodegrdation and hence increases the degradation efficiency [47].
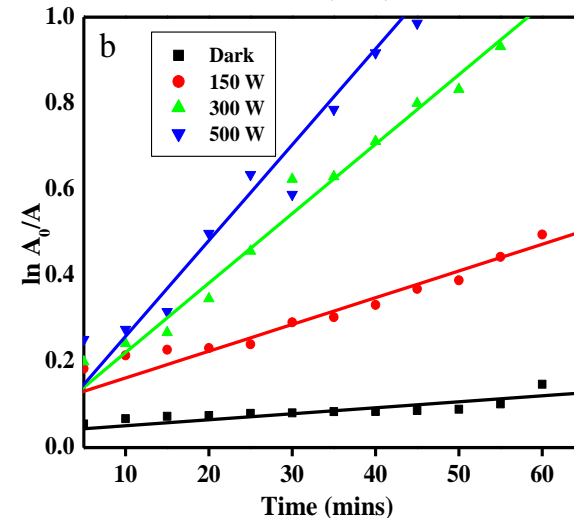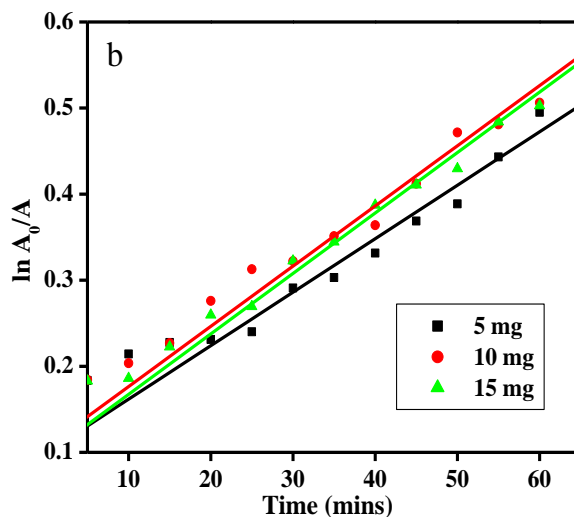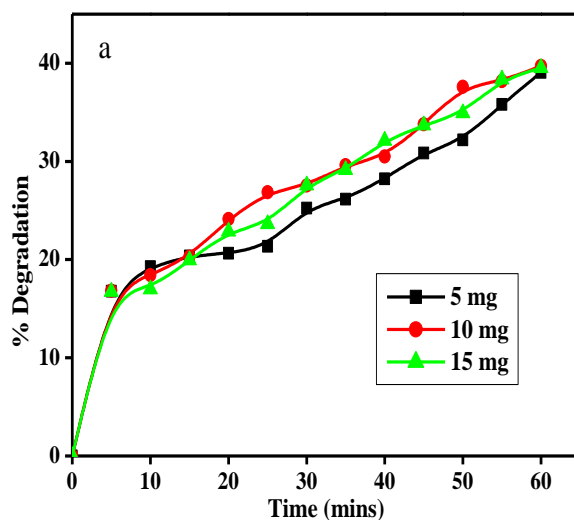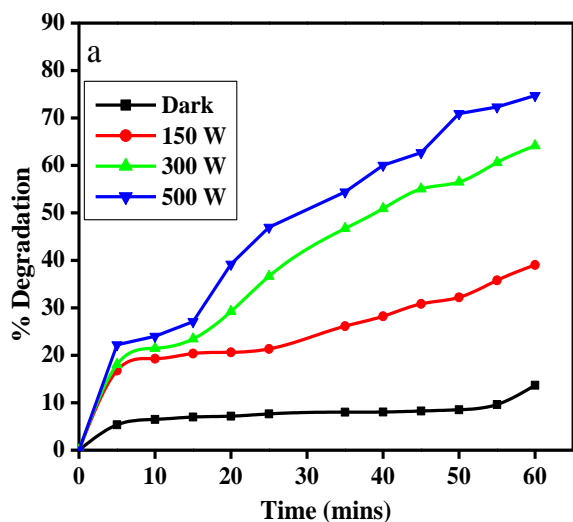

Fig. 10. a) Effect of visible light intensity on degradation of MB, b) Rate of degradation of MB at different visible light ([MB] = 1×10^{-5} M, pH = 6, [H_2O_2] = 5×10^{-3} M, NiO = 0.1 gL^{-1}).

International Journal of Research in Advent Technology, Vol.6, No.11, November 2018
E-ISSN: 2321-9637
Available online at www.ijrat.org

3.6. *Mechanism of photocatalytic activity*

The photocatalytic activity is influenced by some crucial factors like surface area, optical absorption, phase structure and separation efficiency of photo-generated charge carriers. From the experimental results, it is observed that the photocatalytic activity of NiO nanoparticles can be attributed to the semiconductor nanostructure. This makes the charge separation more effective and hence the electrons and holes migrate to the surface of respective particles and participate in the redox reaction. In the reaction mechanism, the photogenerated electrons reduced the dissolved oxygen into peroxide ($O_2^{2-\bullet}$) or hydroxyl ($HO^{\bullet}$) radicals; meanwhile the photo generated holes likely to oxidize H_2O to form HO radicals [48, 49]. The HO radicals from both the process can effectively oxidize MB into minerals as end products.

It is observed that the proportion degradation of MB increases with increase in artificial light intensity and almost 77.79 % MB molecules were decomposed within 60 min at 500 W light intensity (39.05 % at 150 W) In the presence of catalyst. The degradation patterns suggested that the degradation of MB followed a pseudo first order kinetic model and the rate constant could be determined according to the above mentioned rate equation ($\ln C = - kt + \ln C_o$). Many degradation reactions occur simultaneously in the same reaction mixture due to different pathways and the presence of new reaction intermediates that are generated during the degradation process. For this reason to define a reaction rate for all the different processes is extremely difficult. Therefore, the degradation process is normally defined as a pseudo-kinetic reaction. For the photocatalytic process studied in this research, the best type of kinetic reaction adapted is a pseudo-first order reaction. Because the initial concentration of the dye is very small (10^{-5} M), the pseudo-first-order kinetic reaction follows a Langmuir-Hinshelwood mechanism for degradation [50, 51]. The semi logarithmic plots of the concentrations verses time give straight lines, where the slope represents the value of k (reaction rate). For all variations, k values are in the range of 10^{-2} min^{-1}.

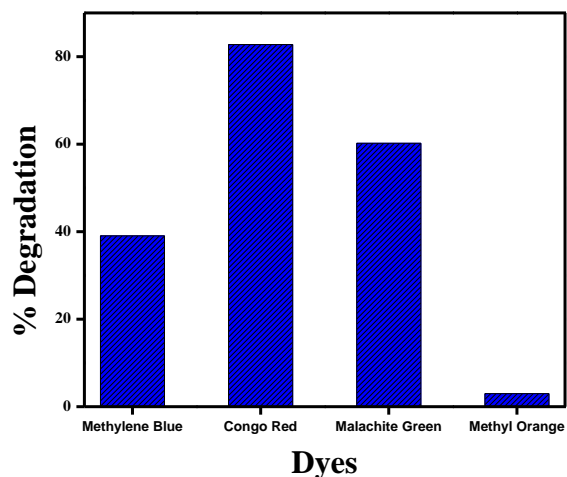### 3.7. *Photocatalytic degradation of different organic dyes*

Fig. 11. Comparative chart of % degradation of different dyes by NiO nanoparticles (pH = 6, [H_2O_2] = 5×10^{-3} M, NiO = 0.1 gL^{-1}, Light intensity = 150W).

In order to confirm the catalytic efficiency, degradation experiments were performed with two cationic such as methylene blue, malachite green, and two anionic dyes such as congo red and methyl orange in the photocatalytic system. From the results it was observed that the degradation rate of methylene blue, malachite green, congo red and methyl orange reached 39.05 %, 60.22 %, 82.43 % and 2.9 % in 60 minutes respectively, at low intensity irradiation (150 W) showed that NiO nanoparticles catalyst has promising photodegradation ability towards various dyes in wastewater.

4. CONCLUSION

In this article, a green, eco-friendly, environmentally benign, facile and cost-effective synthesis of NiO was developed by using *Pisonia alba* leaf extract. The biomolecules present in the extract act as complexing as well as capping agent in the synthesis of NiO nanoparticles. The TEM images and SAED pattern showed the formation of well crystalline NiO nanoparticles with an average particle size of 10-14 nm. XRD and SAED pattern revealed the crystalline structure of NiO nanoparticles. The prepared NPs were employed for the adsorption/degradation of methylene blue (MB) dye in an aqueous medium at pH 6. The maximum catalytic efficiency (77.7%) for the reduction of methylene blue (MB) dye was achieved in a short time span (60 min) at 500 W light intensity. The degradation efficiency was influenced by the solution pH, concentration of H_2O_2, initial dye

International Journal of Research in Advent Technology, Vol.6, No.11, November 2018
E-ISSN: 2321-9637
Available online at www.ijrat.org

concentration, catalyst dosages and light irradiation. The degradation result could be related to the high surface area of the nanostructured catalyst. According with the results presented in this research we can predict that, with high probability, these catalytic processes could be implemented as appropriate chemical procedures for pollutant removal from water.

Acknowledgment

REFERENCES

[1] Wang, X.; Batter, B.; Xie, Y.; Pan, K.; Liao, Y.; Lv, C.; Fu, H. (2015): Highly crystalline, small sized, monodisperse α-NiS nanocrystal ink as an efficient counter electrode for dye-sensitized solar cells. Journal of Materials Chemistry A, **3**(31), pp. 15905-15912.

[2] Ci, S.; Wen, Z.; Qian, Y.; Mao, S.; Cui, S.; Chen, J. (2015): NiO-Microflower formed by nanowire-weaving nanosheets with interconnected Ni-network decoration as supercapacitor electrode. Scientific Reports, **5**(1), pp. 1-12.

[3] Zhu, Y.; Cao, C.; Tao, S.; Chu, W.; Wu, Z.; Li, Y. (2014): Ultrathin Nickel hydroxide and oxide nanosheets: Synthesis, characterizations and excellent supercapacitor performances. Scientific Reports, **4**(1), pp. 1-7.

[4] Shifu, C.; Sujuan, Z.; Wei, L.; Wei, Z. (2008): Preparation and activity evaluation of p–n junction photocatalyst NiO/TiO$_2$. Journal of Hazardous Materials, **155**(1-2), pp. 320-326.

[5] Kumar, R.; Baratto, C.; Faglia, G.; Sberveglieri, G.; Bontempi, E.; Borgese, L. (2015): Tailoring the textured surface of porous nanostructured NiO thin films for the detection of pollutant gases. Thin Solid Films, **583**, pp. 233-238.

[6] Berchmans, S.; Gomathi, H.; Rao, G.P. (1995): Electrooxidation of alcohols and sugars catalysed on a nickel oxide modified glassy carbon electrode. J. Electroanal. Chem., **394**(1-2), pp. 267-270.

[7] Ghosh, M.; Biswas, K.; Sundaresan, A.; Rao, C.N.R. (2006): MnO and NiO nanoparticles: synthesis and magnetic properties. Journal of Materials Chemistry, **16**(1), pp. 106-111.

[8] Deng, X.; Chen, Z. (2004): Preparation of nano-NiO by ammonia precipitation and reaction in solution and competitive balance. Materials Letters, **58**(3-4), pp. 276-280.

[9] Mahaleh, Y.; Sadrnezhaad, S.K.; Hosseini, D. (2008) NiO nanoparticles synthesis by chemical precipitation and effect of applied surfactant on distribution of particle size. Journal of Nanomaterials, **2008** (1), pp.1-4.

[10] Zhu, Z.; Wei, N.; Liu, H.; He, Z. (2011): Microwave-assisted hydrothermal synthesis of Ni(OH)$_2$ architectures and their in situ thermal convention to NiO. Advanced Powder Technology, **22**(3), pp. 422-426.

[11] Zhang, X.; Shi, W.; Zhu J. (2010): Synthesis of porous NiO nanocrystals with controllable surface area and their application as supercapacitor electrodes. Nano Research, **3**(9) pp. 643-652.

[12] Imran Din, M.; Rani, A. (2016): Recent Advances in the Synthesis and Stabilization of Nickel and Nickel Oxide Nanoparticles: A Green Adeptness. International Journal of Analytical Chemistry, **2016**, pp. 1-14.

[13] Patel, R.; Suresh, S. (2006): Decolourization of azo dyes using magnesium-palladium system. J. Hazard. Mater. **137**(3), pp. 1729-1741.

[14] Tian, M.; Dong, C.; Cui, X.; Dong, Z. (2016): Nickel and cobalt nanoparticles modified hollow mesoporous carbon microsphere catalysts for efficient catalytic reduction of widely used dyes, RSC Adv. **6**(101), pp. 99114-99119.

[15] Yu, K.; Zhang, H.; Lv, J.-h.; Gong, L.-h.; Wang, C.-m.; Wang, L.; Wang C.-x.; Zhou, B.-b. (2015): High-efficiency photo- and electro-catalytic material based on a basket-like {Sr$_3$P$_6$Mo$_{18}$O$_{73}$} cage, RSC Adv. **5**(73), pp. 59630-59637.

[16] Tayade, R.J.; Natarajan T.S.; Bajaj, H.C. (2009): Photocatalytic Degradation of Methylene Blue Dye Using Ultraviolet Light Emitting Diodes, Ind. Eng. Chem. Res. **48**(23), pp. 10262-10267.

[17] Laszlo, J.A. (2000): Regeneration of Azo-Dye-Saturated Cellulosic Anion Exchange Resin by *Burkholderia cepacia* Anaerobic Dye Reduction. Environ. Sci. Technol., **34**(1), pp. 167-172.

[18] Liu, J.; Zhang, Q.; Yang, J.; Ma, H.; Tade, M.O.; Wang, S.; Liu, J. (2014), Facile synthesis of carbon-doped mesoporous anatase TiO$_2$ for the enhanced visible-light driven photocatalysis. Chem. Commun., **50**(90), pp. 13971-13974.

[19] Xie, Y.; Yan, B.; Xu, H.; Chen, J.; Liu, Q.; Deng, Y.; Zeng, H. (2014), Highly Regenerable Mussel-Inspired Fe$_3$O$_4$@Polydopamine-Ag Core-Shell Microspheres as Catalyst and Adsorbent for Methylene Blue Removal. ACS Appl. Mater. Interfaces, **6**(11), pp. 8845-8852.

[20] Yagub, M.T.; Sen, T.K.; Afroze, S.; Ang, H.M. (2014): Dye and its removal from aqueous solution by adsorption: a review. Adv. Colloid Interface Sci., **209**, pp. 172-184.

[21] Akkini Devi, T.; Ananthi, N.; Peter Amaladhas, T. (2016): Photobiological synthesis of noble

metal nanoparticles using *Hydrocotyle asiatica* and application as catalyst for the photodegradation of cationic dyes. J. Nanostruct. Chem., **6**, pp. 75-92.

[22] Zhan, H.; Suzuki, T.; Aizawa, K.; Miyagawa, K.; Nagai, R. (2010): Ataxia telangiectasia mutated (ATM)-mediated DNA damage response in oxidative stress-induced vascular endothelial cell senescence. J. Biol. Chem., **285**(38), pp. 29662-29670.

[23] Helen, S.M.; Rani, H.E. (2015): Characterization and antimicrobial study of nickel nanoparticles synthesized from *Dioscorea* (elephant yam) by green route. Int. J. Sci. Res. **4**(11), pp. 216-219.

[24] Arokiyaraj, S.; Arasu, M.V.; Vincent, S.; Prakash, N.U.; Choi, S.H.; Oh, Y.K.; Choi, K.C.; Kim, K.H. (2014): Rapid green synthesis of silver nanoparticles from *Chrysanthemum indicum* L. and its antibacterial and cytotoxic effects: an in vitro study. Int. J. Nanomedicine, **9**, pp. 379-388.

[25] Basak, G.; Das, D.; Das, N. (2014): Dual role of acidic diacetatesophorolipid as biostabilizer for ZnO nanoparticle synthesis and biofunctionalizing agent against *Salmonella enterica* and *Candida albicans*. J. Microbiol. Biotechnol., **24**(1), pp. 87-96.

[26] Kim, S.H.; Umar, A.; Kumar, R.; Ibrahim, A.A.; Kumar, G. (2015): Facile synthesis and photocatalytic activity of cocoon-shaped CuO nanostructures. Mater. Lett., **156**, pp. 138-141.

[27] Qi, X.; Su, G.; Bo, G.; Cao, L.; Liu, W. (2015): Synthesis of NiO and NiO/TiO$_2$ films with electrochromic and photocatalytic activities. Surf. Coat. Technol., **272**, pp. 79-85.

[28] Natarajan, R.K.; Ragothaman, P.; Velachamy, G.; Balakrishna, K. (1990): Chemical examination of *Pisonia grandis*. Bulletin of Medico ethanobotanical research, **11**(4), pp. 110-111.

[29] Duan, W.J.; Lu, S.H.; Wu, Z.L.; Wang, Y.S. (2012): Size Effects on Properties of NiO Nanoparticles Grown in Alkali salts. J. Phys. Chem. C, **116**, pp. 26043-26051.

[30] Le Calvar, M.; Lenglet, M. (1989): Application of Optical Methods (50000-400 cm^{-1}) to Study the Oxidation of Nickel: Theoretical Approach and Experience. Studies in Surface Science and Catalysis, **48**, pp. 567-573.

[31] Helan, V.; Joseph Prince, J.; Al-Dhabi, N.A.; Arasu, M.V.; Ayeshamariam, A.; Madhumitha, G.; Roopan, S.M.; Jayachandran, M. (2016): Neem leaves mediated preparation of NiO nanoparticles and its magnetization, coercivity and antibacterial analysis. Results in Physics, **6**, pp. 712-718.

[32] Angel Ezhilarasi, A.; Judith Vijaya, J.; Kaviyarasu, K.; John Kennedy, L.; Jothi Ramalingam, R.; Al-Lohedan, H.A. (2018): Green synthesis of NiO nanoparticles using *Aegle marmelos* leaf extract for the evaluation of in-vitro cytotoxicity, antibacterial and photocatalytic properties. Journal of Photochemistry & Photobiology, B: Biology, **180**, pp. 39-50.

[33] George, G.; Anandhan, S. (2014): Synthesis and characterisation of nickel oxide nanofibre webs with alcohol sensing characteristics. RSC Adv., **4**(107), pp. 62009-62020.

[34] Adhikary, J.; Chakraborty, P.; Das, B.; Datta, A.; Dash, S.K.; Roy, S., Chen, J.W.; Chattopadhyay, T. (2015): Preparation and characterization of ferromagnetic nickel oxide nanoparticles from three different precursors: application in drug delivery. RSC Advances, **5**(45), pp. 35917-35928.

[35] Ramesh, M.; Rao, M.P.C.; Anandan, S.; Nagaraja, H. (2018): Adsorption and photocatalytic properties of NiO nanoparticles synthesized via a thermal decomposition process. Journal of Materials Research, **33**(05), pp. 601-610.

[36] Pilban Jahromi, S.; Pandikumar, A.; Goh, B.T.; Lim, Y.S.; Basirun, W.J.; Lim, H.N.; Huang, N.M. (2015): Influence of particle size on performance of a nickel oxide nanoparticle-based supercapacitor. RSC Advances, **5**(18), pp. 14010-14019.

[37] Dhal, J.P.; Mishra, B.G.; Hota, G. (2015): Hydrothermal synthesis and enhanced photocatalytic activity of ternary Fe$_2$O$_3$/ZnFe$_2$O$_4$/ZnO nanocomposite through cascade electron transfer. RSC Advances, **5**(71), pp. 58072-58083.

[38] Asiri A.M.: Al-Amoudi M.S.; Al-Talhi T.A.; Al-Talhi A.D. (2009): Photodegradation of Rhodamine 6G and phenol red by nanosized TiO$_2$ under solar irradiation. J. Saudi Chem. Soc. **15**, pp. 121-128.

[39] Willkomm, J.; Orchard, K.L.; Reynal, A.; Pastor, E.; Durrant, J.R.; Reisner, E. (2016): Dye-sensitised semiconductors modified with molecular catalysts for light-driven H2 production. Chemical Society Reviews, **45**(1), pp. 9-23.

[40] Banat, F.; Al-Asheh, S.; Al-Rawashdeh, M.; Nusair, M. (2005): Photodegradation of methylene blue dye by the UV/H$_2$O$_2$ and UV/acetone oxidation processes. Desalination, **181**(1-3), pp. 225-232.

[41] Sridevi, D.; Rajendran, K.V. (2009): Synthesis and optical characteristics of ZnO nanocrystals. Bull. Mater. Sci., **32**(2), pp. 165-168.

[42] Al-Shamali, S.S. (2013): Photocatalytic Degradation of Methylene Blue in the Presence of TiO$_2$ Catalyst Assisted Solar Radiation. Aust. J. Basic Appl. Sci., **7**, pp. 172-176.

[43] Ameta, R.; Sharma, S.; Sharma, S.; Gorana, Y. (2015): Visible Light Induced Photocatalytic Degradation of Toluidine Blue-O by using Molybdenum Doped Titanium Dioxide. European Journal of Advances in Engineering and Technology, **2**, pp. 95-99.

[44] Byrappa, K.; Subramani, A.K.; Ananda, S.; Lokanatha, R.K.M.; Dinesh, R.; (2006):

Photocatalytic degradation of Rhodamine B dye using hydrothermally synthesized ZnO. Bull. Mater. Sci., **29**, pp. 433-438.

[45] Pare, B.; Sarwan, B.; Jonnalagadda, S.B. (2011): Photocatalytic mineralization study of malachite green on the surface of Mn-doped BiOCl activated by visible light under ambient condition. Applied Surface Science, **258**(1), pp. 247-253.

[46] Charanpahari, A.; Ghugal, S.G.; Umare, S.S.; Sasikala, R. (2015): Mineralization of malachite green dye over visible light responsive bismuth doped TiO_2–ZrO_2 ferromagnetic nanocomposites. New Journal of Chemistry, **39**(5), pp. 3629-3638.

[47] Thakur, R.S.; Chaudhary, R.; Singh, C. (2010): Fundamentals and applications of the photocatalytic treatment for the removal of industrial organic pollutants and effects of operational parameters: A review. Journal of Renewable and Sustainable Energy, **2**(4), pp. 042701.

[48] Ge, M.; Li, J.W.; Liu, L.; Zhou, Z. (2011): Template-Free Synthesis and Photocatalytic Application of Rutile TiO_2 Hierarchical Nanostructures. Ind. Eng. Chem. Res. **50**, pp. 6681-6687.

[49] Mu, J.; Shao, C.; Guo, Z.; Zhang, Z.; Zhang, M.; Zhang, P.; Chen, B.; Liu, Y. (2011): High photocatalytic Activity of ZnO-Carbon Nanofiber Hetero architectures. ACS Appl. Mat. Interfaces. **3**, pp. 590-596.

[50] Wang, X.H.; Li, J.G.; Kamiyama, H.; Moriyoshi, Y.; Ishigaki, T. (2006): Wavelength-Sensitive Photocatalytic Degradation of Methyl Orange in Aqueous Suspension over Iron (III)-doped TiO_2 Nanopowders under UV and Visible Light Irradiation. J. Phys. Chem. B, **110**(13), pp. 6804-6809.

[51] Mu, J.; Chen, Zhang, M.; Guo, Z.; Zhang, P.; Zhang, Z.; Sun, Y.; Shao, C.; Liu, Y. (2012): Enhancement of the Visible-Light Photocatalytic Activity of In_2O_3-TiO_2 Nanofiber Heteroarchitectures. ACS Appl. Mat. Interfaces, **4**, pp. 424-430.